Int. J. Exp. Path. (2007), 88, 31–38
doi: 10.1111/j.1365-2613.2006.00514.x

ORIGINAL ARTICLE

Histopathological study of time course changes in inter-renal aortic banding-induced left ventricular hypertrophy of mice

Hiroyuki Higashiyama, Masaki Sugai, Hirotaka Inoue, Kaori Mizuyachi, Hiroshi Kushida, Satoshi Asano and Mine Kinoshita

Pharmacology Department, Tsukuba Research Laboratories, GlaxoSmithKline KK, Ibaraki, Japan

INTERNATIONAL JOURNAL OF EXPERIMENTAL PATHOLOGY

Summary

The left ventricular hypertrophy (LVH) in response to pressure overload is an important risk factor in cardiac morbidity and mortality. To investigate the time course of histopathological alterations in the LVH in response to pressure overload, histopathological and immunohistochemical examination was performed using the aortic banding-induced mouse LVH model. Five-week-old male CD-1 mice were subjected to the inter-renal aortic banding. Major organs were sampled on 3, 10, 14, 21, 28 or 42 days after banding. Haematoxylin and eosin (H&E) staining, Masson's trichrome staining and immunohistochemistry for proliferating cell nuclear antigen (PCNA), alpha-smooth muscle actin (aSMA), ICAM-1, type I collagen and CD31 was performed and microscopically examined. Three days after aortic banding, acute inflammatory changes, such as macrophages/neutrophil infiltration and vascular wall injury were observed on/around the coronary arteries/arterioles of both ventricles. Intense ICAM-1 immunostaining was observed on the endothelium of the coronary arteries/arterioles. After day 10, vascular wall thickening and perivascular fibrosis was induced on the coronary arteries/arterioles. Immunohistochemistry for aSMA and PCNA demonstrated the proliferation of vascular smooth muscle cells in the media. After day 28, minimal cardiomyocyte hypertrophy was observed at the light microscope level. In the inter-renal aortic banding LVH model, histopathological alterations in early phase were mainly observed on coronary arteries/arterioles. These early phase alterations were thought to be hypertension-related changes in the coronary vasculatures. The cardiomyocyte hypertrophy observed in later phase was minimal at the light microscope level. These evidences would facilitate the understanding of pathophysiology of pressure overload LVH.

Keywords
aortic banding, histopathology, left ventricular hypertrophy

Received for publication:
27 September 2006
Accepted for publication:
11 October 2006

Correspondence:
Satoshi Asano
Pharmacology Department
Tsukuba Research Laboratories
GlaxoSmithKline KK
43 Wadai
Tsukuba
Ibaraki 300 4247
Japan
Tel.: +81 29 864 5050
Fax: +81 29 864 8558
E-mail: satoshi.asano@gsk.com

The left ventricular hypertrophy (LVH) in response to pressure overload is a compensatory mechanism to maintain circulatory homeostasis. However, prolonged pressure overload results in excessive cardiomyocyte hypertrophy and fibrosis which lead to increased stiffness and impairment of pumping capacity (Swynghedauw 1999; Fedak *et al.*

2005a,b,c) and would be a risk factor in cardiac morbidity and mortality including heart failure, coronary diseases, sudden death in the patients with hypertension and ventricular dysrhythmias (Levy *et al.* 1987, 1989; Brilla *et al.* 1991; Haider *et al.* 1998). Therefore, prevention or regression of LVH is emerging as a major therapeutic target (Levy *et al.* 1987, 1989; Brilla *et al.* 1991; Haider *et al.* 1998).

The mechanisms underlying the development of pressure overload-induced LVH have been extensively studied using mouse aortic banding models (Wang *et al.* 2004). The transverse or abdominal aortic bonding has been mainly used to mechanically induce cardiac pressure overload (Rockman *et al.* 1991; Wettschureck *et al.* 2001; Esposito *et al.* 2002). With either model, the heart is challenged with an immediate pressure overload and myocardial hypertrophy develops. After aortic banding, there was an initial increase in cardiac contractility with enhanced activity of sympathetic nervous system (Brede *et al.* 2002) and progressive LV enlargement and dysfunction were evident after 8 weeks (Esposito *et al.* 2002).

To date, using aortic banding models, several signal molecules, such as angiotensin II (Baker *et al.* 1990; Kagaya *et al.* 1990), TNF-α (Stamm *et al.* 2001) TGF-β (Takahashi *et al.* 1994; Kuwahara *et al.* 2002), IGF-1 (Donath *et al.* 1998; Tanaka *et al.* 1998) and endothelin-1(Ito *et al.* 1994; Ichikawa *et al.* 1996) have been proposed as mediators promoting pressure overload-induced LVH. In addition, the use of these aortic banding methods in genetically modified animals, such as gene knockout or transgenic, has provided significant insight into the cellular and molecular pathway leading to the development of LVH (Barbosa *et al.* 2005). Moreover, aortic banding models were applied to genome-wide transcriptional profiling or proteomics analysis, and candidate genes involved in the pathophysiology of the cardiac response to pressure overload were identified (Wagner *et al.* 2004; Lindsey *et al.* 2006).

In aortic banding-induced model, we observed the time course of biomarker changes after inter-renal aortic banding such as significant increases in angiotensin II in plasma, and increase in cardiac expression of brain natriuretic peptide (BNP), beta myosin heavy chain (beta-MHC), alpha smooth muscle actin (aSMA) and a decrease in SERCA2 genes [H Inoue (unpublished data)]. These data indicated that increases in gene expression including inflammation, fibrosis and proliferation were induced in response to aortic banding. To further investigate the time course of histopathological alterations after pressure overload, we histopathologically and immunohistochemically examined the inter-renal aortic banding-induced LVH model.

Methods

Animal treatment

Five-week-old male CD-1 mice (23–27 g), purchased from Charles River Japan, were used for the experiment. Animals were housed under controlled environmental conditions with free access to standard laboratory food and water according to Ethical Guideline for Animal Experiments, Tsukuba Research Laboratories, GlaxoSmithKline. The animals were anaesthetized initially with isoflurane (3.5% in medical grade oxygen) in an induction chamber, and maintained at 2% concentration throughout the surgery. After making a sidelong laparotomy, the intestines were reflected and isolation of the abdominal aorta was made between the renal arteries. A 30-gauge injection needle was positioned adjacent to the aorta. To make a fixed stenosis, the aorta and injection needle were ligated by 6-0 silk thread and the needle was immediately removed. The surgical wound was closed in layers and the animals were allowed to recover on a warming pad overnight to maintain normothermia. The sham operation was identical except that the aorta was not ligated.

Tissue sampling and processing

Three, 7, 10, 14, 21 and 42 days after aortic banding, the mice were killed by exsanguination from the abdominal aorta under deep anaesthesia. Isolated heart, kidney, lung, aorta and adrenal glands were fixed in 10% neutral-buffered formalin, embedded in paraffin. Coronal sections (2 μm thickness) were prepared and stained with either haematoxylin–eosin (HE) or Masson's trichrome method.

Immunohistochemistry

Immunohistochemistry was performed using VECTASTAIN elite ABC kit (Vector Laboratories, Burlingame, CA, USA) Briefly, the sections were deparaffinized with xylene and rehydrated through gradient ethanol immersion. Antigen retrieval was performed by microwaving (500 W) the sections for 10 min in citric acid buffer (2 mM citric acid and 9 mM trisodium citrate dehydrate, pH 6.0). After cooling down at room temperature for 20 min, the slides were washed twice in PBS. Endogenous peroxidase activity was quenched by peroxidase blocking reagent (Dako, Glostrup, Denmark) for 7 min, followed by two 1-min washes with PBS. The sections were then blocked with 5% normal sheep serum or normal rabbit serum for 20 min. After two 1-min washes with PBS, sections were incubated with the EPOS^{TM} anti-PCNA/HRP (U7032, Dako), EPOS^{TM} anti-alpha

Smooth Muscle Actin/HRP (Dako), 1/500 dilution of anti-CD31 antibody (Santa Cruz Biotechnology, Santa Cruz, CA, USA) or 1/100 dilution of anti-ICAM-1 antibody (R&D Systems, Minneapolis, MN, USA). Negative control was performed by replacing the primary antibody with mouse IgG or normal goat IgG.

For immunohistochemical detection of CD31 or ICAM-1, specimens were treated with biotinized goat anti-mouse antibody for 20 min at room temperature, and after two 5-min washes with PBS containing 0.02% (v/v) Tween 20 (PBST), the specimens were incubated with streptavidin-horseradish peroxidase for 20 min at room temperature.

After two 1-min washes with PBST, reaction product was visualized with DAB liquid system (Dako) at room temperature for 2 min. Sections were counterstained with haematoxylin for 30 s and rinsed with tap water, immediately dehydrated by sequential immersion in gradient ethanol and xylene, then mounted with Permount on coverslips.

Microscopic evaluation and image acquisition

The sections were evaluated by scanning the entire tissue specimen under low-power magnification (×40) and then confirmed under higher power magnification (×200 and ×400). The severity of histopathological findings was scored as (0) absent, (1) minimal, (2) mild, (3) moderate and (4) marked change. All histopathological scoring and evaluation was carried out by blind evaluation without knowing treatment. Images were obtained under a light microscope (Olympus BX51; Olympus, Tokyo, Japan) equipped with a DP70 digital camera.

Results

After the aortic banding, the following significant histopathological alterations were observed in the heart and kidney. In the sham-operated animal, there was no evidence of histopathological alterations in the examined tissues. The results of the histopathological evaluation are summarized in Table 1.

Inflammatory change

On day 3, a massive cellular infiltration dominated by neutrophils and macrophages was observed was observed on the coronary arteries/arterioles of both ventricles (Figure 1a).

Table 1 Incidence of histopathological findings observed in the heart. Histopathological examination data shown as the number of animals with each score/total number of animals for each time point

Histopathological finding	Grading (score)	Day 3	Day 10	Day 14	Day 21	Day 28	Day 42
Macrophage infiltration	Absent (0)	0/7	1/7	1/7	1/7	1/7	2/7
	Minimal (1)	4/7	4/7	2/7	6/7	4/7	5/7
	Mild (2)	1/7	1/7	3/7	0/7	2/7	0/7
	Moderate (3)	2/7	1/7	1/7	0/7	0/7	0/7
	Marked (4)	0/7	0/7	0/7	0/7	0/7	0/7
Neutrophil infiltration	Absent (0)	0/7	6/7	7/7	7/7	7/7	7/7
	Minimal (1)	4/7	1/7	0/7	0/7	0/7	0/7
	Mild (2)	1/7	0/7	0/7	0/7	0/7	0/7
	Moderate (3)	2/7	0/7	0/7	0/7	0/7	0/7
	Marked (4)	0/7	0/7	0/7	0/7	0/7	0/7
Vascular wall thickening	Absent (0)	7/7	2/7	3/7	2/7	2/7	0/7
	Minimal (1)	0/7	4/7	0/7	1/7	0/7	5/7
	Mild (2)	0/7	0/7	1/7	4/7	3/7	2/7
	Moderate (3)	0/7	1/7	2/7	0/7	1/7	0/7
	Marked (4)	0/7	0/7	1/7	0/7	1/7	0/7
Fibrosis, perivascular	Absent (0)	7/7	3/7	3/7	2/7	2/7	0/7
	Minimal (1)	0/7	4/7	0/7	3/7	2/7	1/7
	Mild (2)	0/7	0/7	4/7	2/7	3/7	0/7
	Moderate (3)	0/7	0/7	0/7	0/7	0/7	0/7
	Marked (4)	0/7	0/7	0/7	0/7	0/7	0/7
Hypertrophy, cardiomyocyte	Absent (0)	7/7	7/7	7/7	7/7	6/7	4/7
	Minimal (1)	0/7	0/7	0/7	0/7	1/7	3/7
	Mild (2)	0/7	0/7	0/7	0/7	0/7	0/7
	Moderate (3)	0/7	0/7	0/7	0/7	0/7	0/7
	Marked (4)	0/7	0/7	0/7	0/7	0/7	0/7

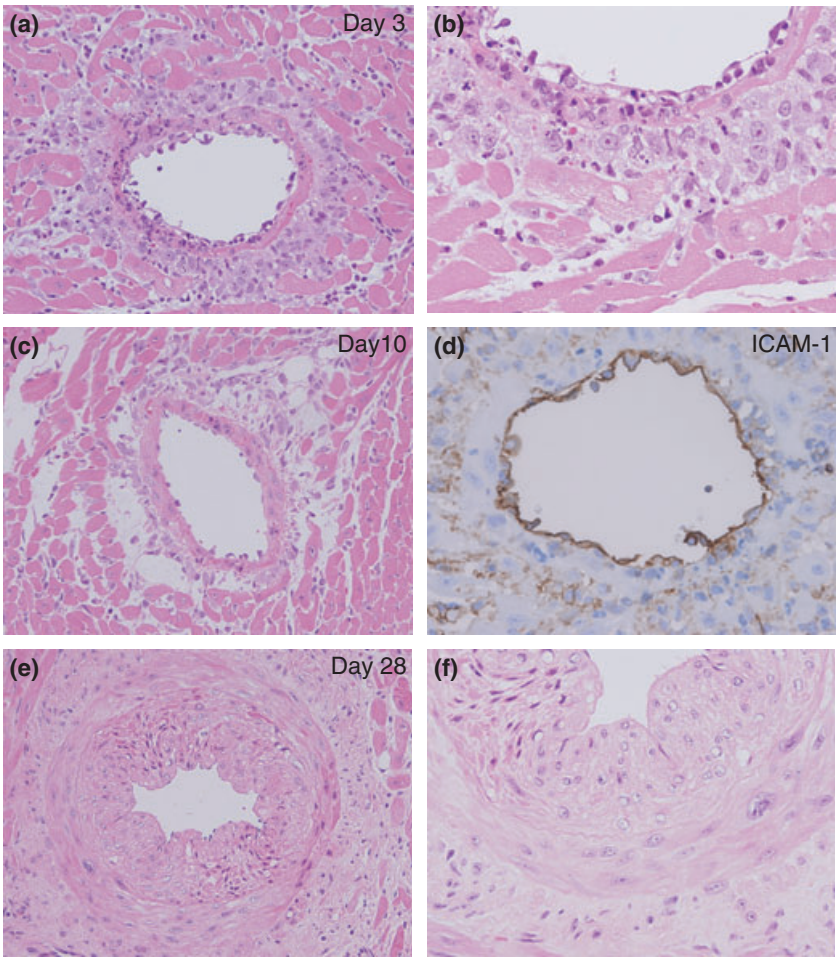

Figure 1 Cellular infiltration and vascular wall thickening observed in the inter-renal aortic banding-induced LVH model. (a) Cellular infiltration dominated by macrophages and neutrophils around coronary artery observed on day 3. (b) Transmigration and infiltration of macrophages/neutrophils observed on day 3. (c) ICAM-1 immunostaining on endothelium of the coronary artery. (d) Mild cellular infiltration dominated around coronary arteries observed on day 10. (e) Moderate coronary artery thickening observed on day 14. HE staining (a, b and d–f), Original magnification ×200 (a, c and e), ×400 (b, d and f).

Transmigration figure of macrophages and vascular injury were frequently observed in coronary arteries (Figure 1b). Immunohistochemistry demonstrated intense ICAM-1 expression localized on the endothelium of coronary arteries/arterioles (Figure 1c). On day 10, the level of neutrophil infiltration significantly declined (Figure 1d), but macrophage infiltration remained at the same level by day 21. After day 21, the level of macrophage infiltration slightly declined.

Vascular wall change

On day 10, a minimal level of vascular wall thickening was observed on coronary arteries/arterioles of both ventricles. On day 14, the level of vascular wall thickening was increased and remained at the same level by day 28 (Figure 1e,f). On day 42, the level of vascular wall thickening slightly decreased.

To identify the cell type contributing to vascular wall thickening, we performed immunohistochemistry of cell type and proliferation markers. CD31, aSMA, type I collagen and PCNA ware used as an endothelial, vascular smooth muscle, fibroblast cell and proliferation maker, respectively. Immunohistochemistry demonstrated an increase in the number of the alpha-smooth muscle actin (aSMA)-positive vascular smooth muscle cells in the media of coronary arteries (Figure 2b). In addition, these vascular smooth muscle cells in thickened arteries showed intense PCNA immunostaining (Figure 2d).

Fibrotic change

On day 10, mild fibroblast proliferation and ECM accumulation in the perivascular area of coronary arteries/arterioles of both ventricles were observed (Figure 1c). On day 14, mild progression of fibroblast proliferation and ECM accumulation was observed, and thereafter it remained at the same level (Figure 3a–d). During the examined time points, fibrotic change was observed relatively limited to the

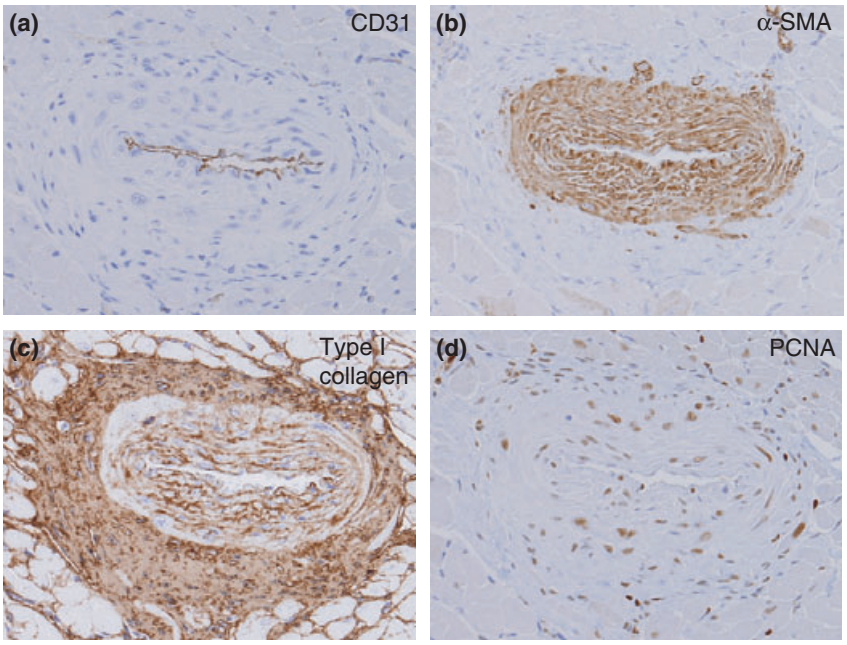

Figure 2 Immunohistochemistry for CD31, aSMA, type I collagen and PCNA in the inter-renal aortic banding-induced LVH model. (a) Endothelium marker, CD31. (b) Vascular smooth muscle cell marker, aSMA. (c) Type I collagen immunostaining. (d) Cell proliferation marker, PCNA. Increase in the number of aSMA-positive vascular smooth muscle cells is observed. PCNA immunostaining preferentially localized to vascular smooth muscle cells. Original magnification ×200 (a–d).

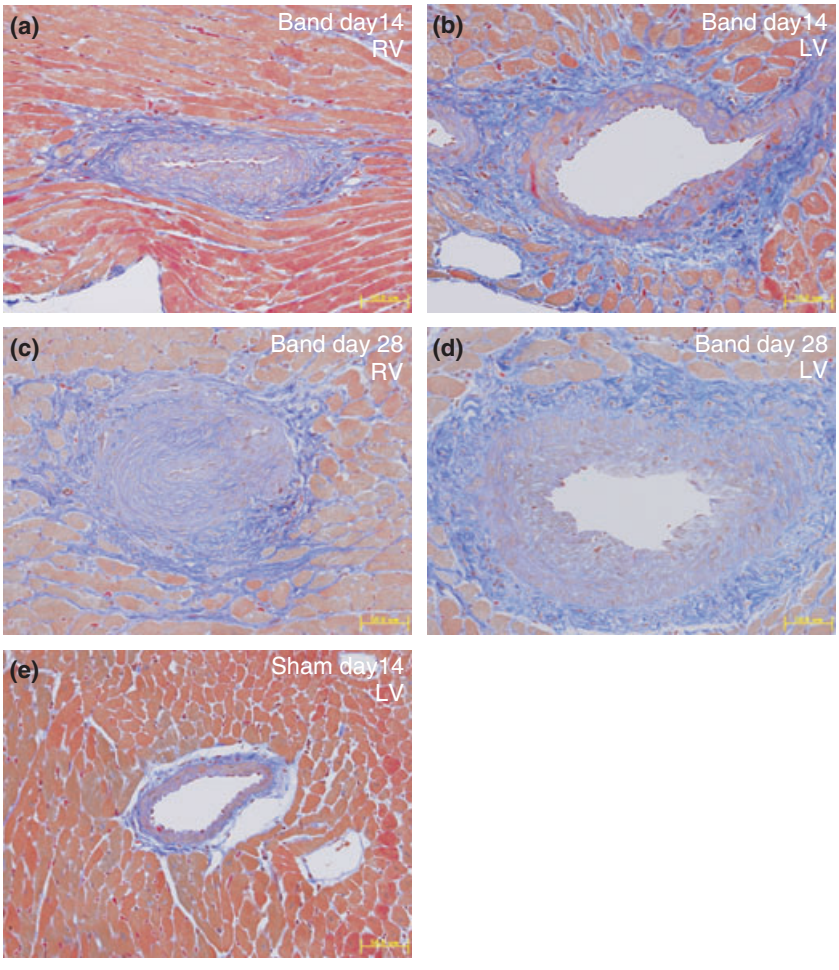

Figure 3 Masson's trichrome staining in the inter-renal aortic banding-induced LVH model. Perivascular fibrosis observed on coronary artery of right ventricle (RV) and left ventricle (LV) at 14 days or 42 days after banding (a and b or c and d respectively). Perivascular area of LV and RV in sham-operated animals on day 14 (e and f) Masson's trichrome staining (a–f). Original magnification ×200 (a–e), bar 50 μm.

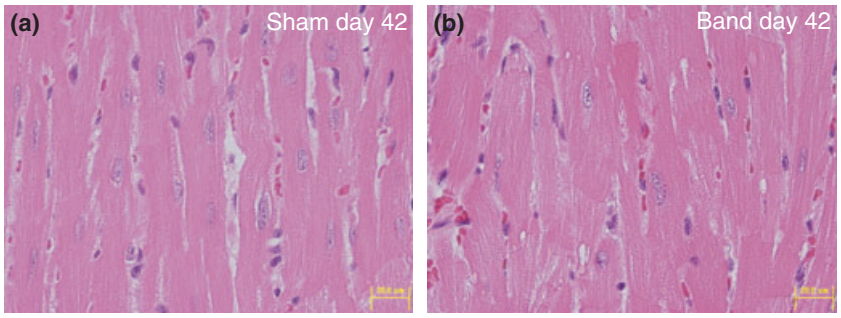

Figure 4 Cardiomyocyte hypertrophy in the inter-renal aortic banding-induced LVH model. (a) Cardiomyocytes of sham-operated animal on day 42. (b) Cardiomyocytes of banded animal on day 42. Note minimal increase in the size of cardiomyocytes in the banded animal. HE staining (a and b), original magnification ×200 (a and b), bar 50 μm.

perivascular area of coronary arteries/arterioles. Increased type I collagen production in the perivascular area was evident by immunohistochemical detection (Figure 2c).

Myocardial hypertrophy

Minimal level of cardiomyocyte hypertrophy was observed on LV after day 28. Slight increase in the size of cardiomyocytes compared with sham-operated animal was observed at the light microscope level (Figure 4a,b). The incidence of cardiomyocyte hypertrophy increased on day 42, although the level of hypertrophy was minimal.

Other findings

In a small number of animals in the banded groups, ischaemia-related kidney changes including cortical atrophy, marked cortical necrosis, interstitial fibrosis and mineralization were observed after day 14 (data not shown).

Discussion

The aortic banding method has been extensively used for the pressure overload LVH model (Wang *et al.* 2004). In the present study, we examined the time course of histopathological alterations in the inter-renal aortic banding-induced LVH model. Histopathological alterations were mainly observed in the heart. Although ischaemia-related renal changes were observed in a small number of banded animals, there was no clear relationship between the severity of heart alterations and atrophied kidney.

Immediate after aortic banding on day 3, acute inflammatory changes including neutrophil/macrophage infiltrations and vascular wall injury were observed. These findings are consistent with the findings in several reports of pressure overload models (Fedak *et al.* 2005a,b), which demonstrated that perivascular inflammation is one of the early phase alterations due to rapid haemodynamic overload against vascular wall or hormonal response. Acute inflammation found in our model was relatively limited to the coronary arteries/arterioles in the heart, not observed on the vasculatures of other examined tissue, suggesting the possibility of temporal local haemodynamic overload on coronary arteries/arterioles rather than systemic change. In the pressure overload rat model, transient upregulation of ICAM-1 was reported to trigger perivascular macrophage accumulation (Kuwahara *et al.* 2003). Consistent with this, we found intense ICAM-1 expression on the endothelium of the coronary arteries/arterioles on days 3 and 10. This result emphasizes the importance of ICMA-1-mediated pathway in cellular infiltration induced by pressure overload.

On day 10, the time point immediately after acute inflammatory phase, perivascular fibrosis and vascular wall thickening were induced. Perivascular fibrosis is one of the key pathological features in the early phase of the hypertensive heart (Kai *et al.* 2005). In the present study, similar to the area of acute inflammation, perivascular fibrosis was relatively limited to coronary arteries/arterioles. This suggests that the perivascular fibrosis observed in this model is a reactive process after acute inflammatory responses. Furthermore, the finding that fibrosis did not progress into the interstitial area during the observation period by day 42 suggests that fibrotic changes in this model did not significantly affect LV function.

In parallel with perivascular fibrosis, vascular wall thickening was observed. Vascular wall thickening was mainly observed on the wall of coronary arteries/arterioles. Immunohistochemistry of aSMA and PCNA clearly revealed prominent proliferation of vascular smooth muscle cells on the media. Proliferation of vascular smooth muscle cells is one of the typical hypertension-related changes in resistant vessels including the coronary artery (Kai *et al.* 2005). Taken together, our data suggested the involvement of

coronary artery/arteriole hypertension in early phase alterations in the heart.

Cardiomyocyte hypertrophy observed in the present study is only minimal at the light microscope level. In a thoracic aortic banding model, cardiomyocyte hypertrophy was more prominent (Rockman *et al.* 1991; Wettschureck *et al.* 2001; Esposito *et al.* 2002). This result is consistent with the general observation that the severity of cardiomyocyte hypertrophy increases when the banding site is closer to the heart.

In conclusion, the present study identified serial histopathological alterations in the heart after inter-renal aortic banding including (i) coronary hypertension-induced vascular injury and acute inflammation, (ii) reactive responses such as perivascular fibrosis and vascular wall thickening, and (iii) minimal cardiomyocyte hypertrophy. These histopathological evidences might facilitate the understanding of the pathophysiology of LVH and contribute to the dosing protocol for anti-LVH drug screening.

Acknowledgements

We thank Ms Miyuki Ito for excellent technical assistance.

References

Baker K.M., Chernin M.I., Wixson S.K., Aceto J.F. (1990) Renin-angiotensin system involvement in pressure-overload cardiac hypertrophy in rats. *Am. J. Physiol.* **259**, H324–H332.

Barbosa M.E., Alenina N., Bader M. (2005) Induction and analysis of cardiac hypertrophy in transgenic animal models. *Methods Mol. Med.* **112**, 339–352.

Brede M., Wiesmann F., Jahns R. *et al.* (2002) Feedback inhibition of catecholamine release by two different alpha2-adrenoceptor subtypes prevents progression of heart failure. *Circulation* **106**, 2491–2496.

Brilla C.G., Janicki J.S., Weber K.T. (1991) Impaired diastolic function and coronary reserve in genetic hypertension. Role of interstitial fibrosis and medial thickening of intramyocardial coronary arteries. *Circ. Res.* **69**, 107–115.

Donath M.Y., Zierhut W., Gosteli-Peter M.A., Hauri C., Froesch E.R., Zapf J. (1998) Effects of IGF-I on cardiac growth and expression of mRNAs coding for cardiac proteins after induction of heart hypertrophy in the rat. *Eur. J. Endocrinol.* **139**, 109–117.

Esposito G., Rapacciuolo A., Naga Prasad S.V. *et al.* (2002) Genetic alterations that inhibit in vivo pressure-overload hypertrophy prevent cardiac dysfunction despite increased wall stress. *Circulation* **105**, 85–92.

Fedak P.W., Verma S., Weisel R.D., Li R.K. (2005a) Cardiac remodeling and failure: from molecules to man (Part II). *Cardiovasc. Pathol.* **14**, 49–60.

Fedak P.W., Verma S., Weisel R.D., Li R.K. (2005b) Cardiac remodeling and failure: from molecules to man (Part I). *Cardiovasc. Pathol.* **14**, 1–11.

Fedak P.W., Verma S., Weisel R.D., Skrtic M., Li R.K. (2005c) Cardiac remodeling and failure: from molecules to man (Part III). *Cardiovasc. Pathol.* **14**, 109–119.

Haider A.W., Larson M.G., Benjamin E.J., Levy D. (1998) Increased left ventricular mass and hypertrophy are associated with increased risk for sudden death. *J. Am. Coll. Cardiol.* **32**, 1454–1459.

Ichikawa K.I., Hidai C., Okuda C. *et al.* (1996) Endogenous endothelin-1 mediates cardiac hypertrophy and switching of myosin heavy chain gene expression in rat ventricular myocardium. *J. Am. Coll. Cardiol.* **27**, 1286–1291.

Ito H., Hiroe M., Hirata Y. *et al.* (1994) Endothelin ETA receptor antagonist blocks cardiac hypertrophy provoked by hemodynamic overload. *Circulation* **89**, 2198–2203.

Kagaya Y., Kanno Y., Takeyama D. *et al.* (1990) Effects of long-term pressure overload on regional myocardial glucose and free fatty acid uptake in rats. A quantitative autoradiographic study. *Circulation* **81**, 1353–1361.

Kai H., Kuwahara F., Tokuda K., Imaizumi T. (2005) Diastolic dysfunction in hypertensive hearts: roles of perivascular inflammation and reactive myocardial fibrosis. *Hypertens. Res.* **28**, 483–490.

Kuwahara F., Kai H., Tokuda K. *et al.* (2002) Transforming growth factor-beta function blocking prevents myocardial fibrosis and diastolic dysfunction in pressure-overloaded rats. *Circulation* **106**, 130–135.

Kuwahara F., Kai H., Tokuda K. *et al.* (2003) Roles of intercellular adhesion molecule-1 in hypertensive cardiac remodeling. *Hypertension* **41**, 819–823.

Levy D., Anderson K.M., Savage D.D., Balkus S.A., Kannel W.B., Castelli W.P. (1987) Risk of ventricular arrhythmias in left ventricular hypertrophy: the Framingham Heart Study. *Am. J. Cardiol.* **60**, 560–565.

Levy D., Garrison R.J., Savage D.D., Kannel W.B., Castelli W.P. (1989) Left ventricular mass and incidence of coronary heart disease in an elderly cohort. The Framingham Heart Study. *Ann. Intern. Med.* **110**, 101–107.

Lindsey M.L., Goshorn D.K., Comte-Walters S. *et al.* (2006) A multidimensional proteomic approach to identify hypertrophy-associated proteins. *Proteomics* **6**, 2225–2235.

Rockman H.A., Ross R.S., Harris A.N. *et al.* (1991) Segregation of atrial-specific and inducible expression of an atrial natriuretic factor transgene in an in vivo murine model of cardiac hypertrophy. *Proc. Natl. Acad. Sci. U.S.A.* **88**, 8277–8281.

Stamm C., Friehs I., Cowan D.B. *et al.* (2001) Inhibition of tumor necrosis factor-alpha improves postischemic recovery of hypertrophied hearts. *Circulation* **104**, I350–I355.

Swynghedauw B. (1999) Molecular mechanisms of myocardial remodeling. *Physiol. Rev.* **79**, 215–262.

Takahashi N., Calderone A., Izzo N.J. Jr, Maki T.M., Marsh J.D., Colucci W.S. (1994) Hypertrophic stimuli induce transforming growth factor-beta 1 expression in rat ventricular myocytes. *J. Clin. Invest.* **94**, 1470–1476.

Tanaka N., Ryoke T., Hongo M. *et al.* (1998) Effects of growth hormone and IGF-I on cardiac hypertrophy and gene expression in mice. *Am. J. Physiol.* **275**, H393–H399.

Wagner R.A., Tabibiazar R., Powers J., Bernstein D., Quertermous T. (2004) Genome-wide expression profiling of a cardiac pressure overload model identifies major metabolic and signaling pathway responses. *J. Mol. Cell Cardiol.* **37**, 1159–1170.

Wang Q.D., Bohlooly M., Sjoquist P.O. (2004) Murine models for the study of congestive heart failure: Implications for understanding molecular mechanisms and for drug discovery. *J. Pharmacol. Toxicol. Methods* **50**, 163–174.

Wettschureck N., Rutten H., Zywietz A. *et al.* (2001) Absence of pressure overload induced myocardial hypertrophy after conditional inactivation of Galphaq/Galpha11 in cardiomyocytes. *Nat. Med.* **7**, 1236–1240.